nature genetics

The stress kinase MKK7 couples oncogenic stress to p53 stability and tumor suppression

Daniel Schramek[1], Athanassios Kotsinas[2], Arabella Meixner[1], Teiji Wada[1], Ulrich Elling[1], J Andrew Pospisilik[1], G Gregory Neely[3], Ralf-Harun Zwick[4], Verena Sigl[1], Guido Forni[5], Manuel Serrano[6], Vassilis G Gorgoulis[2] & Josef M Penninger[1]

Most preneoplastic lesions are quiescent and do not progress to form overt tumors. It has been proposed that oncogenic stress activates the DNA damage response and the key tumor suppressor p53, which prohibits tumor growth. However, the molecular pathways by which cells sense a premalignant state *in vivo* are largely unknown. Here we report that tissue-specific inactivation of the stress signaling kinase MKK7 in KRas^{G12D}-driven lung carcinomas and NeuT-driven mammary tumors markedly accelerates tumor onset and reduces overall survival. Mechanistically, MKK7 acts through the kinases JNK1 and JNK2, and this signaling pathway directly couples oncogenic and genotoxic stress to the stability of p53, which is required for cell cycle arrest and suppression of epithelial cancers. These results show that MKK7 functions as a major tumor suppressor in lung and mammary cancer in mouse and identify MKK7 as a vital molecular sensor to set a cellular anti-cancer barrier.

JNK kinases (JNK1, 2 and 3) are required for cells to respond to their extracellular environment and regulate many physiological processes such as proliferation, apoptosis, differentiation and inflammation[1]. The JNK kinase pathway has also been implicated in tumorigenesis[2]. However, both tumor-promoting and tumor-suppressive functions have been reported[1–8]. Many of the inconsistencies in these data might be due to the fact that the studies used whole-body knockout mice or knock-ins of inactive JNK substrates[3–8]. In such studies, non-cell autonomous functions of JNK, such as inflammatory responses, angiogenesis, stroma interaction or tumor immune surveillance, might contribute to the tumor phenotypes[1,2,5,6]. Furthermore, previous studies have shown that there are functional redundancies and compensation among isoforms of JNK[2]. The kinases MKK4 and MKK7, which are encoded by *Map2k4* and *Map2k7*, respectively, are required for optimal activation of JNKs in a synergistic fashion[9]. However, it has been reported that MKK4 can also affect the second stress kinase pathway p38 (refs. 1,9). Therefore, to target JNK signaling in a tissue-specific and conditional fashion *in vivo*, we focused on MKK7, a specific and essential upstream regulator of the JNK signaling cascade.

RESULTS

Conditional deletion of *Map2k7*

To investigate the role of MKK7 and MKK7-regulated activation of JNK in tumorigenesis, we generated a new mouse line that carries a conditional *Map2k7* (also known as *Mkk7*) allele (*Map2k7^{floxed}*; **Supplementary Fig. 1a** and Online Methods). We confirmed germline transmission by DNA blotting. We removed the *neo* cassette using a Flpe deleter line and confirmed the presence of the remaining *LoxP* sites by sequencing. *Map2k7^{floxed}* mice were viable and fertile and showed no detectable phenotypes. Deletion of *Map2k7* in the epidermis (K5-Cre *Map2k7$^{floxed/floxed}$* mice) resulted in an 'eye-open at birth' (EOB) phenotype (**Supplementary Fig. 1b**,**c**) similar to *Mapk8$^{-/-}$*; *Mapk9$^{+/-}$* (also known as *Jnk1$^{-/-}$*; *Jnk2$^{+/-}$*) compound mutant mice[10] and mice with epidermal deletion of *cJun*[11], a key downstream target of the JNK signaling pathway. Thus, we have generated a *Map2k7^{floxed}* allele that allows tissue-specific inactivation of the MKK7-JNK signaling pathway.

Prolonged survival in MKK7 deficient KRas^{G12D} lung tumors

To test the role of MKK7 in lung cancer driven by the inducible oncogenic KRas^{G12D} allele, we crossed *Map2k7$^{floxed/\Delta}$* mice with a *Lox-Stop-Lox-KRas^{G12D}* strain (termed KRas; *Map2k7$^{fl/\Delta}$* hereafter). *Lox-Stop-Lox-KRas^{G12D}* mice rapidly develop non–small-cell lung carcinomas (NSCLCs) after induction of the KRas^{G12D} allele[12]. We achieved expression of KRas^{G12D} and deletion of exons 3–10 of Map2k7 by adenoviral delivery of Cre recombinase through inhalation (AdCre; **Supplementary Fig. 1d**,**e**). Notably, deletion of *Map2k7* in the KRas^{G12D}-driven model of lung cancer resulted in markedly shortened survival, whereas the mean survival time of littermate controls was 185 days post AdCre infection, the mean survival of KRas; *Map2k7$^{fl/\Delta}$* mice was only 102 days post AdCre infection (**Fig. 1a**). Lung tumors from KRas; *Map2k7$^{fl/\Delta}$* mice showed efficient deletion of *Map2k7* and impaired activation of the JNK-cJun pathway,

[1]Institute of Molecular Biotechnology of the Austrian Academy of Sciences (IMBA), Vienna, Austria. [2]Department of Histology and Embryology, School of Medicine, University of Athens, Athens, Greece. [3]Garvan Institute of Medical Research, Darlinghurst, Sydney, Australia. [4]Department of Respiratory and Critical Care Medicine, Otto Wagner Hospital, Vienna, Austria. [5]Molecular Biotechnology Center, Department of Clinical and Biological Sciences, University of Turin, Turin, Italy. [6]Spanish National Cancer Research Centre (CNIO), Madrid, Spain. Correspondence should be addressed to J.M.P. (josef.penninger@imba.oeaw.ac.at).

Received 1 June 2010; accepted 19 January 2011; published online 13 February 2011; doi:10.1038/ng.767

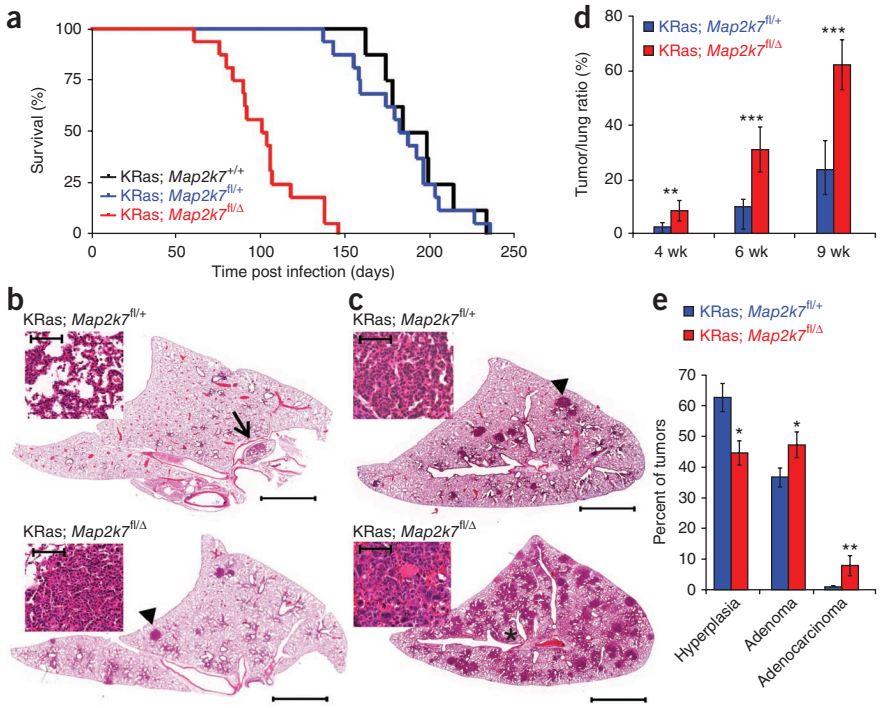

Figure 1 MKK7 controls onset, incidence and progression of KRas^{G12D}-driven lung tumorigenesis. Analysis of lung tumor progression in *Map2k7*$^{+/+}$, *Map2k7*$^{fl/+}$ and *Map2k7*$^{fl/\Delta}$ mice harboring the inducible *Lox-Stop-Lox-KRas*^{G12D} oncogene. We treated the mice with AdCre (2.5×10^7 PFU) and killed them at the indicated time points. (**a**) Survival of mice infected with AdCre depicted by Kaplan Meier blot. $n = 16$ per genotype; $P < 0.0001$ (log rank test for KRas; *Map2k7*$^{+/+}$ versus KRas; *Map2k7*$^{fl/\Delta}$ and KRas; *Map2k7*$^{fl/+}$ versus KRas; *Map2k7*$^{fl/\Delta}$). (**b**,**c**) Representative sections (stained with hematoxylin and eosin) showing accelerated progression and increased tumor burden in KRas; *Map2k7*$^{fl/\Delta}$ mice 4 weeks (**b**) and 6 weeks (**c**) after AdCre infection. Insets show the highest grade lesion in each lung. Arrow indicates the hyperplastic region. Arrowheads indicate adenomas. The asterisk marks an adenocarcinoma. Magnifications are ×40. (**d**) Average tumor-to-lung area at the indicated time points after AdCre infection. At least three planes from each lung were stained with hematoxylin and eosin and analyzed in a blinded fashion. Data are shown as means ± s.e.m. At least eight mice per genotype and time point were analyzed. (**e**) Distribution of hyperplasia, adenomas and adenocarcinomas in KRas; *Map2k77*$^{fl/+}$ and KRas; *Map2k7*$^{fl/\Delta}$ littermates 6 weeks after AdCre infection. For quantification, we combined hyperplastic lesions and atypical adenomatous hyperplasia (AAH). Data are shown as means ± s.e.m. ($n = 12$ per genotype). Magnifications are ×10. $^*P < 0.05$; $^{**}P < 0.01$; $^{***}P < 0.001$ (Student's *t*-test). Scale bars, 10 μm for insets and 2 mm for whole-lung pictures.

whereas the levels of expression of MKK4 and total JNK proteins were unchanged (**Supplementary Fig. 1f**,**g**). Notably, the expression and phosphorylation of p38, ERK1, ERK2 and AKT were not impaired in MKK7-deficient lung tumors; rather, these pathways were slightly upregulated (**Supplementary Fig. 1f**). Thus, MKK7 functions as a tumor suppressor in KRas^{G12D}-induced lung cancer.

MKK7 controls tumor onset of KRas^{G12D}-driven lung cancer

We next monitored tumor onset at early stages after AdCre infection. Whereas at 4 weeks after infection only 20% of control KRas; *Map2k7*$^{fl/+}$ mice ($n = 10$) developed hyperplasia, all KRas; *Map2k7*$^{fl/\Delta}$ mice ($n = 9$) harbored multiple hyperplastic lesions and even solid adenomas at this point (**Fig. 1b** and **Supplementary Fig. 2a**). Six weeks after AdCre inhalation, we again observed markedly increased numbers of solid adenomas as well as the formation of adenocarcinomas in the lungs of KRas; *Map2k7*$^{fl/\Delta}$ mice (**Fig. 1c** and **Supplementary Fig. 2a**). Because of the large size of lung adenocarcinomas at 9 weeks after tumor initiation, we could not count individual tumors in KRas; *Map2k7*$^{fl/\Delta}$ mice at this time point (**Supplementary Fig. 2a**,**b**). Quantification of overall tumor burden confirmed a significant increase at all time points in KRas; *Map2k7*$^{fl/\Delta}$ mice compared to KRas; *Map2k7*$^{fl/+}$ control littermates (**Fig. 1d**). These results show that deletion of *Map2k7* facilitates KRas^{G12D}-driven initiation and growth of lung cancer.

We next classified the progression of lung tumors 6 weeks after tumor initiation as previously described[13] (**Supplementary Fig. 3a**). KRas; *Map2k7*$^{fl/\Delta}$ mice contained significantly more adenocarcinomas than did littermate controls (**Fig. 1e**). Moreover, staining for the proliferation marker Ki67 showed that lung tumors in KRas; *Map2k7*$^{fl/\Delta}$ mice underwent increased proliferation in the hyperplastic regions (4 weeks after AdCre infection) as well as in solid adenomas (6 weeks after AdCre infection; **Supplementary Fig. 3b**). We did not detect apoptotic cells in KRas^{G12D}-induced lung lesions from littermate control or KRas; *Map2k7*$^{fl/\Delta}$ mice (**Supplementary Fig. 3c**); this finding is in line with previous studies and is probably due to the fact that oncogenic KRas^{G12D} is a potent inhibitor of apoptosis[14]. Thus, these data show that MKK7 not only controls tumor initiation but also suppresses malignant progression.

Mapk8$^{+/-}$*; Mapk9*$^{-/-}$ mice exhibit enhanced lung tumor growth

MKK7, with MKK4, is essential for phosphorylating and activating JNKs. In the lung, JNK1 and JNK2, but not JNK3, are expressed[1]. We therefore investigated whether the identified tumor-suppressive functions are mediated by JNK1, JNK2 or both and generated KRas^{G12D} mice that carried mutations in *Mapk8* (also known as *Jnk1*) or *Mapk9* (also known as *Jnk2*). Loss of *Mapk8* alone or inactivation of *Mapk9* did not affect tumor burden or overall survival during KRas^{G12D}-mediated lung tumorigenesis (**Fig. 2a** and **Supplementary Fig. 4a**,**b**). *Mapk8*; *Mapk9* double-knockout mice die as embryos[10]; however, compound *Mapk8*$^{-/-}$; *Mapk9*$^{+/-}$ (*Jnk1*$^{-/-}$; *Jnk2*$^{+/-}$) mice have been used to unmask phenotypes such as eyelid closure defects[10]. We therefore tested KRas^{G12D}-induced lung tumorigenesis in such compound mutant animals. Both *Mapk8*$^{+/-}$; *Mapk9*$^{-/-}$ and *Mapk8*$^{-/-}$; *Mapk9*$^{+/-}$ compound mutants were born at Mendelian ratios and survived into adulthood. We found no obvious phenotype in adult *Mapk8*; *Mapk9* compound mutant mice except the previously reported eyelid closure defect in *Mapk8*$^{-/-}$; *Mapk9*$^{+/-}$ mice, which was absent from *Mapk8*$^{+/-}$; *Mapk9*$^{-/-}$ mutants[10]. During KRas^{G12D}-induced lung tumorigenesis *Mapk8*$^{+/-}$; *Mapk9*$^{-/-}$, but not *Mapk8*$^{-/-}$; *Mapk9*$^{+/-}$, compound mutants showed accelerated tumor growth and progression compared to littermate controls (**Fig. 2a**,**b**). Protein blotting of total lung lysates showed that *Mapk8*$^{-/-}$; *Mapk9*$^{+/-}$ mice expressed near-normal levels of total JNK (**Supplementary Fig. 4c**). By contrast, JNK expression was severely compromised in lungs

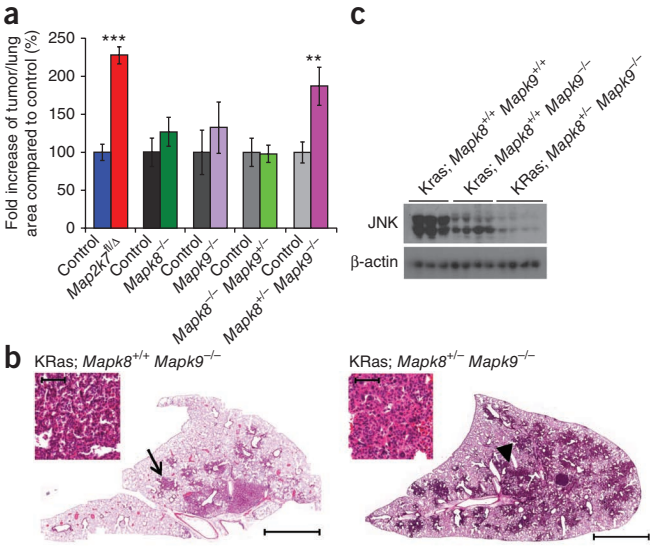

Figure 2 *Mapk8*$^{+/-}$; *Mapk9*$^{-/-}$ compound mutant mice phenocopy the effect of MKK7 deletion. Genetic dissection of JNK isoform functions in KRas^{G12D}-driven lung tumors. (**a**) Analysis of tumor burden in *Mapk8*$^{-/-}$ (*JNK1*$^{-/-}$), *Mapk9*$^{-/-}$ (*JNK2*$^{-/-}$) and *Mapk8/9* compound mutant mice reveals increased tumor-to-lung area in *Mapk8*$^{+/-}$; *Mapk9*$^{-/-}$ but not in *Mapk8*$^{-/-}$ single, *Mapk9*$^{-/-}$ single or *Mapk8*$^{-/-}$; *Mapk9*$^{+/-}$ mice. We analyzed the lungs 9 weeks after AdCre infection. Changes are given as fold increases compared to control littermates (control). Data are shown as means ± s.e.m. $^{**}P < 0.01$; $^{***}P < 0.001$ (Student's *t*-test). (**b**) Representative sections (stained with hematoxylin and eosin) of KRas; *Mapk8*$^{+/+}$; *Mapk9*$^{-/-}$ and KRas; *Mapk8*$^{+/-}$; *Mapk9*$^{-/-}$ littermates 9 weeks after AdCre infection. Insets show an adenoma in a KRas; *Mapk8*$^{+/+}$; *Mapk9*$^{-/-}$ mouse (arrow) and an adenocarcinoma in a KRas; *Mapk8*$^{+/-}$; *Mapk9*$^{-/-}$ mouse (arrowhead). Magnifications are ×40. (**c**) Expression of JNK and p53 in *Mapk8*$^{+/-}$; *Mapk9*$^{-/-}$ compound mutant KRas^{G12D}-induced tumors. β-actin is shown as loading control. An overexposed blot for total JNK is presented to show residual total JNK expression in lung tumors of *Mapk8*$^{+/-}$; *Mapk9*$^{-/-}$ compound mutant mice. Scale bars, 100 μm for insets and 2 mm for whole-lung pictures.

from *Mapk8*$^{+/-}$; *Mapk9*$^{-/-}$ compound mutant mice (**Fig. 2c**), indicating that JNK2 is the major isoform in the lung or that JNK2 can compensate for the loss of JNK in lung tumors. These data show that the MKK7-JNK1/2 signaling axis acts as a tumor suppressor pathway in KRas^{G12D}-induced lung cancer.

MKK7 deficiency affects the DNA damage response

How does the MKK7-JNK1/2 pathway suppress epithelial tumorigenesis? We used gene expression profiling to define the molecular mechanisms of MKK7-mediated tumor suppression. As MKK7 affects the early stages in tumor development, we decided to use primary pneumocytes from KRas; *Map2k7*$^{fl/+}$ and KRas; *Map2k7*$^{fl/\Delta}$ littermates rather than transformed cells from established tumors that may harbor additional, secondary mutations. Immunohistochemical analysis confirmed the presence of SP-C–expressing type II pneumocytes and low numbers of CC10-expressing Clara cells in the primary pneumocyte culture, mirroring the prevalent cell types in tumors that arose in the KRas^{G12D}-driven tumor model (**Supplementary Fig. 5a**,**b**), confirming previous data[12]. We cultured pneumocytes for 3 days and infected them with Ad-Cre-GFP to induce expression of the KRas^{G12D} oncogene and the concomitant deletion of *Map2k7* (**Supplementary Fig. 6a**). Microarray analysis (GEO accession number GSE26763) and Gene Set Enrichment Analysis (GSEA) revealed that genes annotated to 'DNA damage response by p53', 'mitotic cell cycle checkpoint' and 'DNA integrity checkpoint' were markedly enriched in KRas^{G12D}-expressing control cells as compared with KRas^{G12D}-expressing MKK7-deficient pneumocytes (**Fig. 3a** and **Supplementary Fig. 6b**). Recent studies have shown that the DDR can be activated by oncogenic stress in early tumor lesions and induces an anti-cancer barrier by activating the H2AX-CHK2-p53 pathway[15–17]. We therefore investigated whether deletion of *Map2k7* has an effect on the DDR-p53 pathway in the KRas^{G12D}-induced lung tumor model, in which tumor induction can be temporally controlled through delivery of the Ad-Cre virus.

Monitoring phosphorylation of histone H2AX (γ-H2AX) and activation of the DNA checkpoint kinase CHK2 revealed that the DNA damage checkpoint cascade is activated in lung premalignant lesions as early as 4 weeks after KRas^{G12D} induction (**Fig. 3b**). The DDR was also induced in adenomas at 6 and 8 weeks after AdCre challenge (**Supplementary Fig. 7a**). Furthermore, we found 53BP1 foci and γH2AX foci in tumor cells, whereas such foci were not visible in adjacent normal pneumocytes (**Supplementary Fig. 7b**).

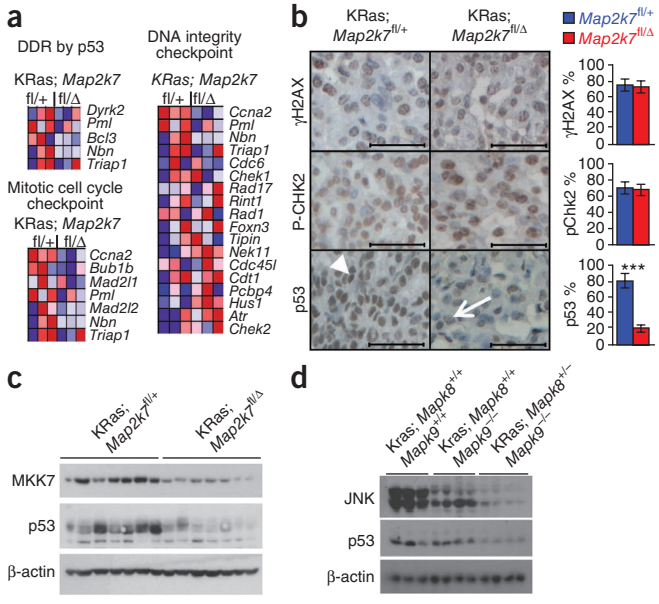

Figure 3 The MKK7-JNK pathway controls p53 expression in lung cancer. (**a**) Gene profiling of primary pneumocytes from KRas; *Map2k7*$^{fl/+}$ and KRas; *Map2k7*$^{fl/\Delta}$ mice treated with AdCre *in vitro*. We used gene set enrichment analysis to determine whether a defined set of genes or pathways showed statistically significant enrichment. All datasets will be published online at NCBI. (**b**) Immunohistochemical analysis of γH2AX, pCHK2 and p53 in premalignant lesions 4 weeks after AdCre infection. Magnifications are ×400. Staining for γH2AX and pCHK2 in hyperplastic lesions from KRas; *Map2k7*$^{fl/+}$ and KRas; *Map2k7*$^{fl/\Delta}$ mice was comparable. Whereas 80% of pneumocytes in adenomas of KRas; *Map2k7*$^{fl/+}$ mice showed intense nuclear p53 immunostaining, only 20% of pneumocytes in hyperplastic regions of KRas; *Map2k7*$^{fl/\Delta}$ mice showed nuclear p53 staining. Furthermore, p53 staining was more intense in hyperplastic lung lesions from control KRas; *Map2k7*$^{fl/+}$ (arrowhead) than from KRas; *Map2k7*$^{fl/\Delta}$ mice (thin arrow). The bar graphs denote percentage of cells positive for γH2AX, pCHK2 and p53. Data are shown as means ± s.e.m. $^{***}P < 0.001$ (Student's *t*-test). (**c**,**d**) Protein blot analysis of p53, MKK7 and total JNK in *Map2k7*-deficient (**c**) and *Mapk8*$^{+/-}$; *Mapk9*$^{-/-}$ compound mutant (**d**) KRas^{G12D}-driven lung tumors 6 weeks after AdCre infection. Data from individual tumors isolated from different mice are shown. Scale bars, 50 μm.

There were no alterations in oncogenic stress-induced activation of γ-H2AX and CHK2 or formation of 53BP1 foci and γH2AX foci in MKK7 mutant lung hyperplasias (**Fig. 3b**) or in solid adenomas (**Supplementary Fig. 7a**,**b**). There was a significant reduction in p53 protein in MKK7-deficient lung hyperplasias 4 weeks after induction of $KRas^{G12}$ (**Fig. 3b**). Not only was the number of p53-positive cells markedly reduced in MKK7-deficient lung lesions compared to hyperplastic regions in littermate controls, but also the staining intensity was decreased in the remaining few p53-positive cells in lungs of KRas; *Map2k7*$^{fl/\Delta}$ mice.

Protein blotting and immunohistochemistry confirmed that p53 was also markedly decreased in all MKK7-deficient adenocarcinomas analyzed 6 and 8 weeks after induction of $KRas^{G12D}$ (**Fig. 3c** and **Supplementary Fig. 7c**). The residual MKK7 band in lungs of KRas; *Map2k7*$^{fl/\Delta}$ mice might represent residual MKK7 in the stroma (fibroblasts, vascular cells and so on) of the isolated tumors or incomplete deletion. Moreover, in *Mapk8*$^{+/-}$; *Mapk9*$^{-/-}$ mice that develop enhanced lung cancer, but not in *Mapk8*$^{-/-}$; *Mapk9*$^{+/-}$ compound mutant mice which had no altered tumorigenesis (**Fig. 2a**), p53 was also decreased (**Fig. 3d**). We did not observe any differences in *p53* mRNA expression among MKK7-expressing and MKK7-deficient $KRas^{G12D}$-driven lung tumors (**Supplementary Fig. 7d**).

As Ras promotes oncogene-induced senescence (OIS) by activating CHK2 *in vitro* and *in vivo*[18–20], we further investigated senescence in our MKK7-deficient $KRas^{G12D}$-driven lung tumors. We found markedly decreased staining of the senescence-associated markers $p16^{INK4A}$ and HP1γ, indicating that senescence was decreased in MKK7-deficient tumors (**Fig. 4a**). There was also a concomitant increase in proliferation as determined by pronuclear cell nuclear antigen (PCNA) staining (**Fig. 4a**). These data indicate that that loss of MKK7 has no apparent effect on transcription of the *Tp53* gene but rather regulates p53 protein stability *in vivo*, which influences oncogene-induced cellular senescence.

MKK7 deficiency affects p53 protein stability

We next wanted to test whether endogenous, oncogenic $KRas^{G12D}$ directly induced DNA damage and influenced p53 expression through MKK7. We therefore isolated primary pneumocytes from *Lox-Stop-Lox-KRas*^{G12D} mice, infected these cells with Ad-GFP or Ad-Cre-GFP to activate $KRas^{G12D}$ and followed the appearance of 53BP1 foci and induction of γH2AX. Notably, we found that endogenous activation of oncogenic $KRas^{G12D}$ did not itself significantly increase the DDR above baseline activity normally found in cultured cells, nor did it significantly increase p53 levels (**Supplementary Fig. 8a**,**b**). This finding is consistent with evidence that endogenous $KRas^{G12V}$ is potent enough neither to transform cells directly nor to cause DDR[21,22]. However, we did observe a trend toward increased formation of 53BP1 foci ($P = 0.097$) as well as slightly increased activation of Erk signaling and proliferation in cells harboring activated $KRas^{G12D}$ compared to control cells treated only with Ad-GFP (**Supplementary Fig. 8b**,**c**). Therefore, the DDR seen in primary tumors is probably largely due to a second hit in $KRas^{G12D}$-driven tumors, as previously reported[23,24].

We decided to model the DDR using genotoxic stress in human A549 cells, which are derived from a non–small-cell lung cancer, express wild-type p53 and carry a mutation in the KRas oncogene in the same amino acid as in our mouse lung cancer model[25]. We treated the cells with doxorubicin, a commonly used chemotherapeutic drug, to trigger double-stand breaks and thereby trigger the DDR and induce p53 (ref. 26). Doxorubicin induced fast and sustained JNK activation in A549 cells dependent on MKK7 expression (**Supplementary Fig. 9a**). Control A549 cells showed strong upregulation of p53 expression after doxorubicin treatment, whereas *Mkk7* knockdown cells showed delayed and less sustained p53 expression (**Fig. 4b**). Consequently, *Mkk7* knockdown cells failed to arrest at the G2/M cell cycle checkpoint after DNA damage (**Supplementary Fig. 9b**). Mechanistically, knockdown of *Mkk7* did not affect *p53*

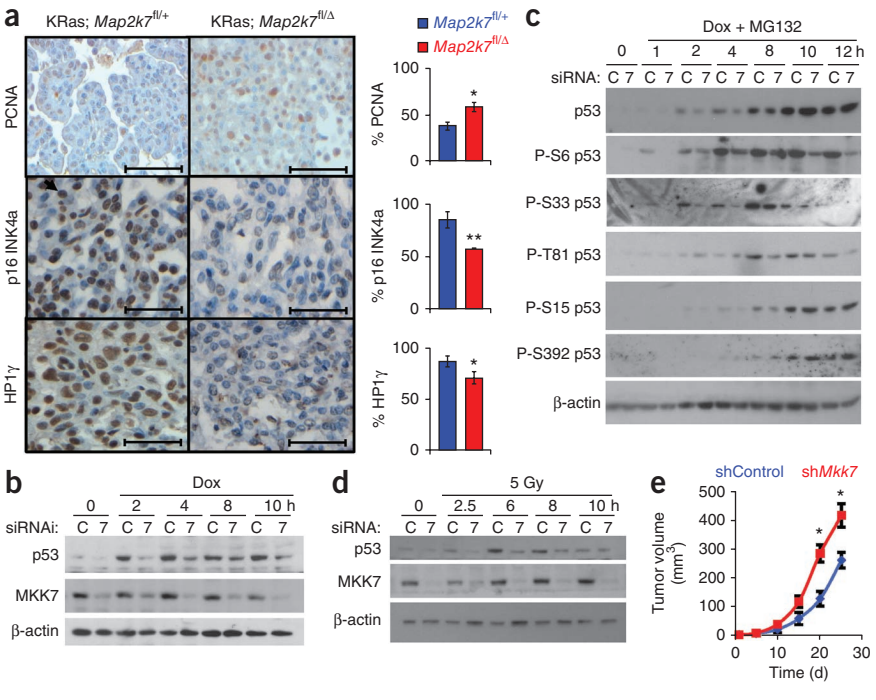

Figure 4 MKK7 regulates senescence and p53 stability. (**a**) Immunohistochemical analysis of PCNA, $p16^{INK4a}$ and HP1γ in adenomas 6 weeks after AdCre infection. The bar graphs show the percentage of cells positive for PCNA, $p16^{INK4a}$ and γHP1. Data are shown as means ± s.e.m. $^*P < 0.05$; $^{**}P < 0.01$ (Student's *t*-test). Magnifications are ×400. (**b**) p53 expression in the human lung tumor cell line A549 after short interfering RNA (siRNA)-mediated knockdown of *Mkk7* and treatment with doxorubicin (Dox; 1 μM). MKK7 and β-actin levels are indicated. C indicates scrambled control cells treated with scrambled siRNA and 7 denotes *Mkk7*-specific siRNA. (**c**) Protein blot analysis of p53 and various phosphorylated (P) forms of p53 after knockdown of *Mkk7* and treatment with doxorubicin (Dox; 1 μM). We used the proteasome inhibitor MG132 (30 μM) to ensure equal p53 levels. β-actin is shown as loading control. (**d**) Protein blot analysis of p53 in A549 cells after siRNA-mediated knockdown of *Mkk7*. Cells were exposed to 5 Gy of γ-irradiation. (**e**) Effect of stable *Mkk7* knockdown using shRNA in A549 lung tumor cells to form xenograft tumors. We injected 5×10^6 A549 cells transfected with pSIREN shScramble or *shMkk7* into nude mice and monitored tumor formation over 26 days. Data are shown as means ± s.e.m. $^*P < 0.05$ (Student's *t*-test). Scale bars, 50 μm.

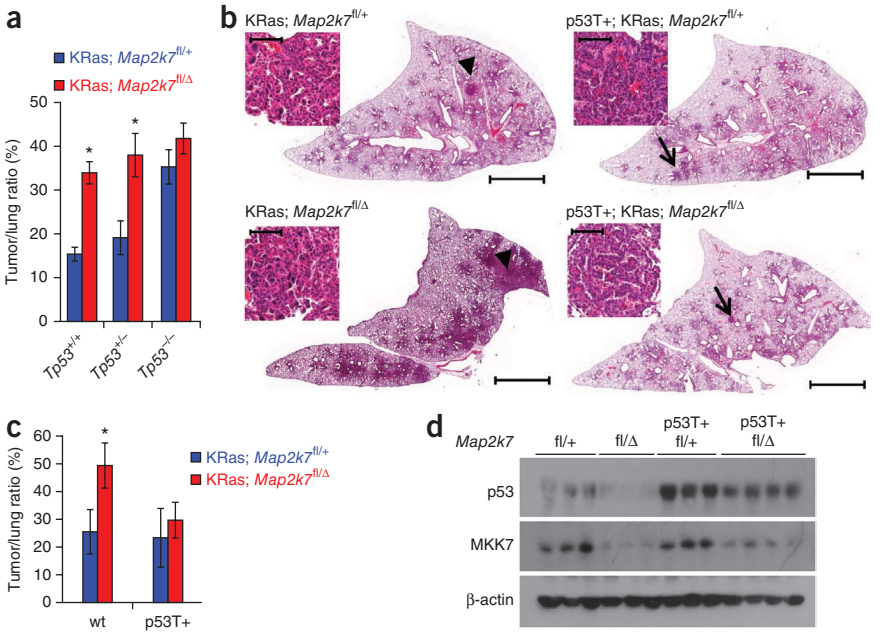

Figure 5 Loss of MKK7 can be rescued by overexpression of p53. (**a**) Genetic inactivation of *Map2k7* on a *Tp53*$^{-/-}$ background does not further increase lung tumor burden. Average tumor-to-lung area is shown 6 weeks after AdCre infection. At least three planes from each lung were stained with hematoxylin and eosin and analyzed in a blinded fashion. At least eight mice per genotype were analyzed. Data are shown as means ± s.e.m. (**b**–**d**) Rescue of MKK7 tumor suppressive function by overexpression of p53. (**b**) Representative histology of littermate control and KRas; *Map2k7*$^{fl/\Delta}$ mice harboring an extra copy of p53 analyzed 9 weeks after AdCre infection. Insets show adenocarcinomas (arrowheads) in KRas; *Map2k7*$^{fl/+}$ and KRas; *Map2k77*$^{fl/\Delta}$ mice and adenomas (arrows) in p53T+; KRas; *Map2k7*$^{fl/+}$ and p53T+; KRas; *Map2k7*$^{fl/\Delta}$ mice. Magnification is ×40. (**c**) Tumor burden 9 weeks after AdCre infection is reduced to control levels in p53T+; KRas; *Map2k7*$^{fl/\Delta}$ mice. We analyzed at least eight mice per genotype. Data are shown as means ± s.e.m. (**d**) Protein blot analysis shows increased p53 in tumors of p53T+; KRas; *Map2k7*$^{fl/\Delta}$ mice. *$P < 0.05$ (Student's *t*-test). Scale bars, 100 μm for insets and 2 mm for whole-lung pictures.

mRNA expression (**Supplementary Fig. 9c**); rather, in the presence of the proteasome inhibitor MG132, we observed comparable induction and expression of *p53* in both *Mkk7* knockdown and control A549 cells (**Fig. 4c**).

To test whether this also holds true for genotoxic injuries other than doxorubicin, we tested γ-irradiation. Again, expression of p53 was delayed and less sustained after γ-irradiation in A549 cells after *Mkk7* knockdown than in control cells (**Fig. 4d**).

MKK7 deficiency affects p53 phosphorylation

The JNK pathway has been implicated as both a positive and a negative regulator of p53. For instance, it has been proposed that JNK targets p53 for degradation in non-stressed cells[27], MEFs lacking JNK1/2 transcriptionally upregulate *p53* mRNA[28] and cJun functions as a potent transcriptional suppressor of p53 (ref. 29). Moreover, deletion of c-Jun in adult mouse liver leads to a decrease in the induction of tumors by carcinogens that results from upregulation of p53 (ref. 30). Thus, one would expect that inactivation of the JNK pathway would result in upregulation of p53. By contrast, *in vitro* JNK can phosphorylate p53 on key residues (Ser6, Ser33 and Thr81) in its N terminus and thereby lead to increased stability[31–33]. Whether this is functionally relevant *in vivo* has not been determined. This prompted us to analyze the phosphorylation status of p53 after genotoxic stress. Knockdown of *Mkk7* in A549 cells led to reduced phosphorylation of p53 on Ser6, Ser33 and, less strongly, Thr81 after treatment with doxorubicin and in the presence of the proteasome inhibitor MG132 to ensure equal p53 levels (**Fig. 4c**). Phosphorylation of p53 on Ser15 or Ser392, sites that are regulated by other kinases such as ATM, ATR, DNA-PK, CDK5 and CDK9, was unaffected[17] (**Fig. 4c**). These data show that the MKK7-JNK pathway couples genotoxic stress to phosphorylation and stability of p53.

Effect of *Mkk7* knockdown on human lung cancer cells

To test the effect of *Mkk7* knockdown in tumor formation by A549 cells, we established stable pools of pSIREN-mediated *Mkk7* knockdown cells and vector control cells (**Supplementary Fig. 9d**). *Mkk7* knockdown cells showed a significant growth advantage over vector control A549 cells after xenografting into nude mice (**Fig. 4e**). Thus, knockdown of *Mkk7* in human A549 lung tumor cells affects p53 protein stability and results in enhanced tumor formation.

To test whether MKK7-JNK signaling is also perturbed in human primary lung tumors, we analyzed MKK7 in samples from human samples. Phosphorylation of MKK7 was upregulated in NSCLCs compared to surrounding healthy tissue. Furthermore, tumors in which p53 was mutated (confirmed by sequencing) showed even higher phosphorylation of MKK7 than did tumors harboring wild-type p53 (**Supplementary Fig. 9e**). Thus, MKK7 is activated in primary human lung tumors and such hyperactivation seems to depend on p53 status.

p53 overexpression reverts lung tumorigenesis

To provide direct evidence that p53 deregulation is indeed functionally relevant for MKK7-mediated tumor suppression *in vivo*, we crossed KRas; *Map2k7*$^{fl/\Delta}$ mice to *Tp53*$^{-/-}$ mice. As previously reported, *Tp53* heterozygosity did not impinge on lung tumor growth[34]. *Tp53* knockout mice showed accelerated lung cancer progression similar to KRas; *Map2k7*$^{fl/\Delta}$ mice (**Fig. 5a** and **Supplementary Fig. 10a**). These data are in line with previous reports showing that deletion of *Tp53* in KRas^{G12}-driven lung tumor results in increased multiplicity and accelerated malignant progression[14,34,35]. Notably, loss of p53 in KRas; *Map2k7*$^{fl/\Delta}$ mice did not further accelerate tumor growth, which is consistent with an epistatic effect between MKK7 and p53 (**Fig. 5a** and **Supplementary Fig. 10a**). However, there were more adenocarcinomas in *Tp53*$^{-/-}$; KRas; *Map2k7*$^{fl/\Delta}$ mice (**Supplementary Fig. 10b**), indicating that loss of p53 does not affect tumor burden on a MKK7-deficient background but results in increased numbers of adenocarcinomas.

To test the hypothesis that p53 levels are crucial for the tumor suppressor activity of MKK7, we crossed KRas; *Map2k7*$^{fl/\Delta}$ animals with 'Super p53' BAC transgenic mice, which harbor an extra copy of p53. We speculated that increasing the p53 gene dose might rescue MKK7 deficiency. Indeed, the p53 transgene (p53T^{+}) markedly reduced the tumor burden in KRas; *Map2k7*$^{fl/\Delta}$ mice to levels found in control mice (**Fig. 5b**,**c**). In the lung tumors of Super 53 transgenic mice,

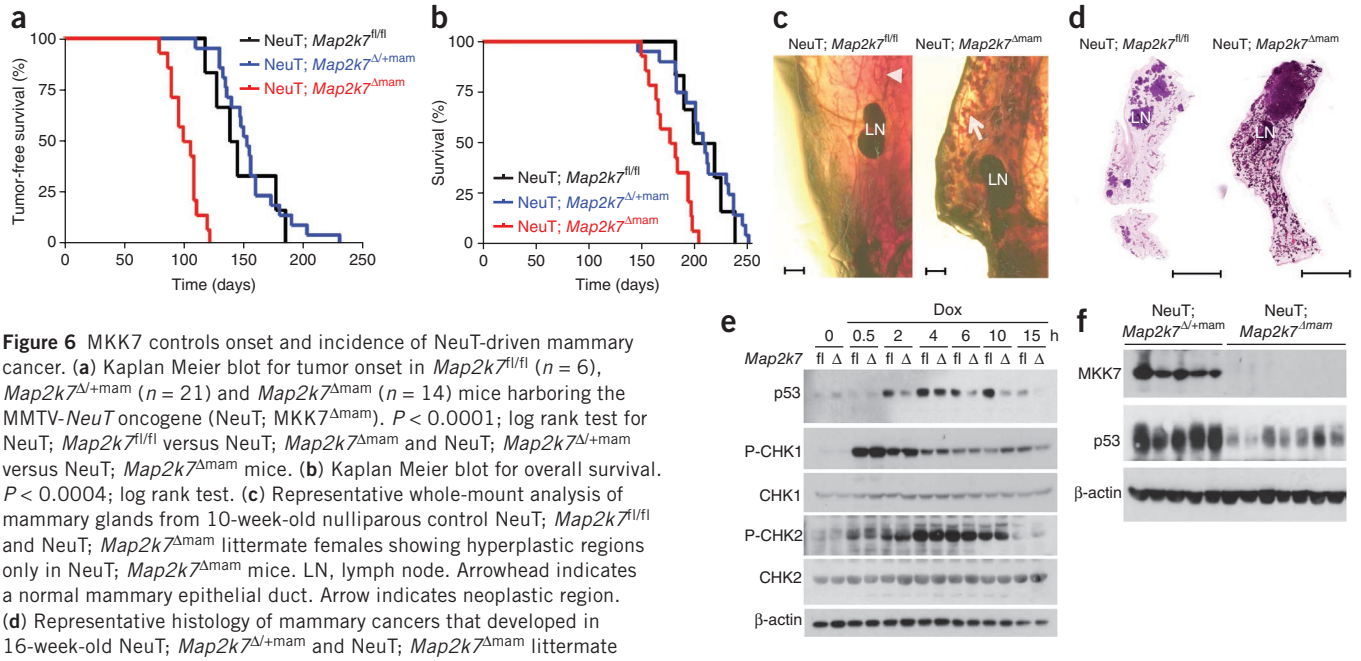

Figure 6 MKK7 controls onset and incidence of NeuT-driven mammary cancer. (**a**) Kaplan Meier blot for tumor onset in *Map2k7*$^{fl/fl}$ ($n = 6$), *Map2k7*$^{\Delta/+mam}$ ($n = 21$) and *Map2k7*$^{\Delta mam}$ ($n = 14$) mice harboring the MMTV-*NeuT* oncogene (NeuT; MKK7$^{\Delta mam}$). $P < 0.0001$; log rank test for NeuT; *Map2k7*$^{fl/fl}$ versus NeuT; *Map2k7*$^{\Delta mam}$ and NeuT; *Map2k7*$^{\Delta/+mam}$ versus NeuT; *Map2k7*$^{\Delta mam}$ mice. (**b**) Kaplan Meier blot for overall survival. $P < 0.0004$; log rank test. (**c**) Representative whole-mount analysis of mammary glands from 10-week-old nulliparous control NeuT; *Map2k7*$^{fl/fl}$ and NeuT; *Map2k7*$^{\Delta mam}$ littermate females showing hyperplastic regions only in NeuT; *Map2k7*$^{\Delta mam}$ mice. LN, lymph node. Arrowhead indicates a normal mammary epithelial duct. Arrow indicates neoplastic region. (**d**) Representative histology of mammary cancers that developed in 16-week-old NeuT; *Map2k7*$^{\Delta/+mam}$ and NeuT; *Map2k7*$^{\Delta mam}$ littermate females (sections stained with hematoxylin and eosin). (**e**) Analysis of p53 activation in primary mammary epithelial cells purified from *Map2k7*$^{fl/fl}$ mice and treated *in vitro* with AdGFP and AdCre to generate *Map2k7*$^{fl/fl}$ (fl) and *Map2k7*$^{\Delta/\Delta}$ (Δ) cells. Protein blot analysis of p53, phosphorylated (P) CHK1, CHK1, phosphorylated (P) CHK2 and CHK2 at different time points after doxorubicin treatment (Dox; 1 μM). β-actin is shown as loading control. (**f**) Protein blot analysis of p53 and MKK7 levels in NeuT-driven breast tumors. β-actin is shown as loading control. Scale bars, 1 mm (**c**) and 5 mm (**d**).

p53 levels were markedly increased, although still lower in MKK7-deficient tumors (**Fig. 5d**). These data provide direct evidence that MKK7 exerts its tumor suppressive function through p53.

MKK7 suppresses NeuT-driven mammary cancer

We next wanted to test whether this finding holds true for another epithelial tissue. To assess the function of stress kinase signaling in epithelial tumorigenesis, we deleted *Map2k7* in mammary epithelial cells using a MMTV-Cre deleter mouse. MMTV-Cre *Map2k7*$^{floxed/\Delta}$ mice (termed *Map2k7*$^{\Delta mam}$ mice hereafter) were viable and healthy and showed normal mammary gland formation throughout puberty and lactation (**Supplementary Fig. 11a** and data not shown). MKK7 is highly expressed in ductal epithelial cells of the mammary gland (**Supplementary Fig. 11b**). Ductal epithelial cells *in situ* (**Supplementary Fig. 11b**), as well as isolated primary mammary epithelial cells (MECs), showed almost complete deletion of MKK7 (**Supplementary Fig. 11c**,**d**). Moreover, primary MECs isolated from *Map2k7*$^{\Delta mam}$ mice showed impaired activation of JNK and cJun in response to the cytotoxic drug anisomycin or the proinflammatory cytokine TNFα (**Supplementary Fig. 11e**).

To test whether inactivation of MKK7 had an effect on mammary tumorigenesis, we crossed *Map2k7*$^{\Delta mam}$ mice with MMTV-*NeuT* transgenic mice, a genetic model of breast cancer, to generate MMTV-*NeuT*; *Map2k7*$^{\Delta mam}$ mice (termed NeuT; *Map2k7*$^{\Delta mam}$ mice hereafter). As in the KRas^{G12D} lung tumor model, we observed a much earlier onset of mammary tumors in NeuT; *Map2k7*$^{\Delta mam}$ mice than in MMTV-*NeuT* mice (**Fig. 6a**). Moreover, the overall survival of NeuT; *Map2k7*$^{\Delta mam}$ female mice was markedly reduced compared to that of control littermates (**Fig. 6b**). Histopathological analysis revealed that these late-stage tumors in both NeuT; *Map2k7*$^{\Delta mam}$ and control mice were typical adenocarcinomas (**Supplementary Fig. 12a**). Whole-mount analysis of mammary glands of 10-week-old mice (before the appearance of any palpable tumors) showed that NeuT; *Map2k7*$^{\Delta mam}$ mice had numerous hyperplastic regions (**Fig. 6c**). At the same time point, we found no such hyperplastic lesions in control littermates (**Fig. 6c**). At 16 weeks of age, the entire mammary fat pad contained hundreds of adenocarcinomas in NeuT; *Map2k7*$^{\Delta mam}$ mice, whereas the mammary fat pads of control mice contained only a few lesions (**Fig. 6d**). These results show that deletion of *Map2k7* in MECs facilitates NeuT-driven cancer formation; that is, MKK7 functions as a potent tumor suppressor in the mammary gland.

MKK7 controls p53 protein stability in MECs

We next isolated primary MECs from *Map2k7*$^{fl/fl}$ mice. We infected these cells with Ad-GFP or Ad-Cre-GFP to delete *Map2k7* and treated them with doxorubicin. Doxorubicin induced fast and sustained MKK7-dependent activation of JNK in primary MECs (**Supplementary Fig. 13a**). As expected, control MECs showed strong activation of the DDR checkpoint kinases CHK1 and CHK2 as well as upregulation of p53 expression after doxorubicin treatment (**Fig. 6e**). However, although MKK7-deficient cells showed apparently normal activation of CHK1 and CHK2, these MECs showed delayed and less sustained p53 protein expression (**Fig. 6e**). Consequently, MKK7-deficient MECs failed to arrest at the G2/M cell cycle checkpoint after DNA damage (**Supplementary Fig. 13b**). Moreover, MKK7-deficient cells failed to induce p53-responsive genes such as *p21, Puma, Mdm2* and *Gadd45γ* (**Supplementary Fig. 13c**).

Mechanistically, loss of MKK7 did not affect *p53* mRNA expression (**Supplementary Fig. 13d**); rather, in the presence of the proteasome inhibitor MG132, we observed comparable induction and expression of p53 in both MKK7-deficient and MKK7-expressing MECs (**Supplementary Fig. 13e**). Similar to our lung cancer model, p53 protein levels, but not mRNA levels, were markedly reduced in all primary MKK7-deficient NeuT-driven mammary tumors analyzed, whereas expression and phosphorylation of p38 did not seem to be affected in breast cancer epithelium (**Fig. 6f**

and **Supplementary Fig. 13f,g**). Thus, loss of MKK7 in mammary epithelial cells does not affect transcription of the *Tp53* gene but directly affects the stability of p53 protein.

DISCUSSION

Most pre-cancerous lesions, such as hyperplasia of the lung and the breast, are quiescent and do not progress to form overt tumors[36,37]. The mechanism of how cells sense their premalignant state and undergo cell cycle arrest and/or cell death is unclear. *In vitro*, oncogenic stimulation of DNA replication can lead to double-strand breaks, stalled DNA forks, allelic imbalance at 'fragile sites', telomere dysfunction or production of reactive oxygen species, all of which will trigger the DDR and p53-dependent cell cycle arrest, senescence and cell death[15–17,19]. In line with this concept, immunohistochemical studies have shown that early human lesions of the lung, breast, skin, colon and bladder show activation of DDR and upregulation of p53 (refs. 15,16). Moreover, activated JNK signaling and the importance of the JNK upstream activator Rac1 in have been described in $KRas^{G12D}$-driven tumors[38,39], but the functional importance of activated JNK signaling has not been addressed. We now confirm that the DDR acts as an anti-tumor barrier in an inducible lung cancer model *in vivo* and identify MKK7-JNK signaling as a crucial component that senses oncogenic stress and thereby links the DDR to p53 stability and tumor suppression (**Supplementary Fig. 14**). However, we cannot rule out the possibility that the oncogene itself or stromal factors such as cytokines participate to activate MKK7-JNK signaling. Further studies are required to elucidate how oncogenic stress is sensed by MKK7 and how ARF[14,17,35,40], ATM[22] and ATR[17] might be involved in MKK7-mediated stabilization of p53.

Activating mutations in *KRAS* (10–30%) and loss-of-function point mutations in *TP53* (50–70%) are frequently found in human non–small-cell lung cancer, whereas 30% of human breast tumors overexpress Her2 (Neu) and about 40% harbor p53 mutations[36,41]. Our genetic *in vivo* data now clearly show that tissue-specific inactivation of MKK7 resulted in impaired p53 protein expression and early onset tumor formation in $K\text{-}Ras^{G12D}$-driven lung carcinomas and NeuT-driven breast cancer. Moreover, we also observed enhanced skin tumors in K5-Cre $Map2k^{fl/fl}$ mice following challenge with the chemical carcinogen DMBA/TPA (data not shown). These *in vivo* data show that the stress kinase MKK7 functions as a tumor suppressor for epithelial cancers of the lung, mammary gland and skin downstream of various oncogenes. Our data might also provide a molecular mechanism by which common genotoxic therapies such as doxorubicin or γ-irradiation, which are used in everyday clinical practice, function as anti-cancer therapies. They also provide support for a re-evaluation of JNK inhibitors as therapeutic strategies for inflammatory and fibrotic diseases, as inhibition of the MKK7-JNK pathway *in vivo* might lead to deregulation of the key tumor suppressor p53.

METHODS

Methods and any associated references are available in the online version of the paper at http://www.nature.com/naturegenetics/.

Accession numbers. Transcriptional profiling of control and MKK7-deficient primary mouse pneumocytes after oncogenic KRasG12 induction was done in biological triplicates. Microarray data and description of experimental design are deposited under GEO number GSE26763.

Note: Supplementary information is available on the Nature Genetics website.

ACKNOWLEDGMENTS

We thank all members of our laboratories for discussions; H. Scheuch and M. Radolf for microarray support; and E. Wagner for reading the manuscript. D.S. is supported by the EU INFLA-CARE network. J.M.P. is supported by grants from IMBA, the Austrian Ministry of Sciences, the Austrian Academy of Sciences, GEN-AU (AustroMouse) and an EU ERC Advanced Grant. V.G.G. and A.K. are supported by the EU-grants INFLA-CARE and GENICA.

AUTHOR CONTRIBUTIONS

D.S. designed and performed most experiments. A.K. and V.G.G. performed the DNA damage and p53 immunohistochemistry and analysis. A.M. performed all RT-PCR analyses. T.W. generated the $MKK7^{floxed}$ mice. U.E. and V.S. helped with immunohistochemistry. R.-H.Z. analyzed the tumor section as the expert pathologist. J.A.P. and G.G.N. helped in microarray and gene set enrichment analysis. G.F. and M.S. contributed to the characterization of the ErbB-2 and Super p53 transgenic mice, respectively. J.M.P. coordinated the project and wrote the manuscript with D.S.

COMPETING FINANCIAL INTERESTS

The authors declare no competing financial interests.

Published online at http://www.nature.com/naturegenetics/.
Reprints and permissions information is available online at http://npg.nature.com/reprintsandpermissions/.

1. Weston, C.R. & Davis, R.J. The JNK signal transduction pathway. *Curr. Opin. Cell Biol.* **19**, 142–149 (2007).
2. Wagner, E.F. & Nebreda, A.R. Signal integration by JNK and p38 MAPK pathways in cancer development. *Nat. Rev. Cancer* **9**, 537–549 (2009).
3. Chen, N. *et al.* Suppression of skin tumorigenesis in c-Jun NH(2)-terminal kinase-2-deficient mice. *Cancer Res.* **61**, 3908–3912 (2001).
4. She, Q.B., Chen, N., Bode, A.M., Flavell, R.A. & Dong, Z. Deficiency of c-Jun-NH(2)-terminal kinase-1 in mice enhances skin tumor development by 12-O-tetradecanoylphorbol-13-acetate. *Cancer Res.* **62**, 1343–1348 (2002).
5. Behrens, A., Jochum, W., Sibilia, M. & Wagner, E.F. Oncogenic transformation by ras and fos is mediated by c-Jun N-terminal phosphorylation. *Oncogene* **19**, 2657–2663 (2000).
6. Kennedy, N.J. *et al.* Suppression of Ras-stimulated transformation by the JNK signal transduction pathway. *Genes Dev.* **17**, 629–637 (2003).
7. Nateri, A.S., Spencer-Dene, B. & Behrens, A. Interaction of phosphorylated c-Jun with TCF4 regulates intestinal cancer development. *Nature* **437**, 281–285 (2005).
8. Sancho, R. *et al.* JNK signalling modulates intestinal homeostasis and tumourigenesis in mice. *EMBO J.* **28**, 1843–1854 (2009).
9. Tournier, C. *et al.* MKK7 is an essential component of the JNK signal transduction pathway activated by proinflammatory cytokines. *Genes Dev.* **15**, 1419–1426 (2001).
10. Weston, C.R. *et al.* The c-Jun NH2-terminal kinase is essential for epidermal growth factor expression during epidermal morphogenesis. *Proc. Natl. Acad. Sci. USA* **101**, 14114–14119 (2004).
11. Zenz, R. *et al.* c-Jun regulates eyelid closure and skin tumor development through EGFR signaling. *Dev. Cell* **4**, 879–889 (2003).
12. Jackson, E.L. *et al.* Analysis of lung tumor initiation and progression using conditional expression of oncogenic K-ras. *Genes Dev.* **15**, 3243–3248 (2001).
13. Nikitin, A.Y. *et al.* Classification of proliferative pulmonary lesions of the mouse: recommendations of the mouse models of human cancers consortium. *Cancer Res.* **64**, 2307–2316 (2004).
14. Fisher, G.H. *et al.* Induction and apoptotic regression of lung adenocarcinomas by regulation of a K-Ras transgene in the presence and absence of tumor suppressor genes. *Genes Dev.* **15**, 3249–3262 (2001).
15. Gorgoulis, V.G. *et al.* Activation of the DNA damage checkpoint and genomic instability in human precancerous lesions. *Nature* **434**, 907–913 (2005).
16. Bartkova, J. *et al.* DNA damage response as a candidate anti-cancer barrier in early human tumorigenesis. *Nature* **434**, 864–870 (2005).
17. Meek, D.W. Tumour suppression by p53: a role for the DNA damage response? *Nat. Rev. Cancer* **9**, 714–723 (2009).
18. Collado, M. *et al.* Tumour biology: senescence in premalignant tumours. *Nature* **436**, 642 (2005).
19. Bartkova, J. *et al.* Oncogene-induced senescence is part of the tumorigenesis barrier imposed by DNA damage checkpoints. *Nature* **444**, 633–637 (2006).
20. Di Micco, R. *et al.* Oncogene-induced senescence is a DNA damage response triggered by DNA hyper-replication. *Nature* **444**, 638–642 (2006).
21. Guerra, C. *et al.* Tumor induction by an endogenous K-ras oncogene is highly dependent on cellular context. *Cancer Cell* **4**, 111–120 (2003).
22. Efeyan, A. *et al.* Limited role of murine ATM in oncogene-induced senescence and p53-dependent tumor suppression. *PLoS ONE* **4**, e5475 (2009).
23. Ding, L. *et al.* Somatic mutations affect key pathways in lung adenocarcinoma. *Nature* **455**, 1069–1075 (2008).
24. Zhang, Z. *et al.* Wildtype Kras2 can inhibit lung carcinogenesis in mice. *Nat. Genet.* **29**, 25–33 (2001).

25. Lehman, T.A. *et al.* p53 mutations, ras mutations, and p53-heat shock 70 protein complexes in human lung carcinoma cell lines. *Cancer Res.* **51**, 4090–4096 (1991).
26. Aas, T. *et al.* Specific P53 mutations are associated with *de novo* resistance to doxorubicin in breast cancer patients. *Nat. Med.* **2**, 811–814 (1996).
27. Fuchs, S.Y. *et al.* JNK targets p53 ubiquitination and degradation in nonstressed cells. *Genes Dev.* **12**, 2658–2663 (1998).
28. Das, M. *et al.* Suppression of p53-dependent senescence by the JNK signal transduction pathway. *Proc. Natl. Acad. Sci. USA* **104**, 15759–15764 (2007).
29. Schreiber, M. *et al.* Control of cell cycle progression by c-Jun is p53 dependent. *Genes Dev.* **13**, 607–619 (1999).
30. Eferl, R. *et al.* Liver tumor development. c-Jun antagonizes the proapoptotic activity of p53. *Cell* **112**, 181–192 (2003).
31. Hu, M.C., Qiu, W.R. & Wang, Y.P. JNK1, JNK2 and JNK3 are p53 N-terminal serine 34 kinases. *Oncogene* **15**, 2277–2287 (1997).
32. Buschmann, T. *et al.* Jun NH2-terminal kinase phosphorylation of p53 on Thr-81 is important for p53 stabilization and transcriptional activities in response to stress. *Mol. Cell. Biol.* **21**, 2743–2754 (2001).
33. Oleinik, N.V., Krupenko, N.I. & Krupenko, S.A. Cooperation between JNK1 and JNK2 in activation of p53 apoptotic pathway. *Oncogene* **26**, 7222–7230 (2007).
34. Jackson, E.L. *et al.* The differential effects of mutant p53 alleles on advanced murine lung cancer. *Cancer Res.* **65**, 10280–10288 (2005).
35. Ji, H. *et al.* LKB1 modulates lung cancer differentiation and metastasis. *Nature* **448**, 807–810 (2007).
36. Herbst, R.S., Heymach, J.V. & Lippman, S.M. Lung cancer. *N. Engl. J. Med.* **359**, 1367–1380 (2008).
37. Costa, A. & Zanini, V. Precancerous lesions of the breast. *Nat. Clin. Pract. Oncol.* **5**, 700–704 (2008).
38. Zhou, Y. *et al.* Chimeric mouse tumor models reveal differences in pathway activation between ERBB family- and KRAS-dependent lung adenocarcinomas. *Nat. Biotechnol.* **28**, 71–78 (2010).
39. Kissil, J.L. *et al.* Requirement for Rac1 in a K-ras induced lung cancer in the mouse. *Cancer Res.* **67**, 8089–8094 (2007).
40. Young, N.P. & Jacks, T. Tissue-specific p19Arf regulation dictates the response to oncogenic K-ras. *Proc. Natl. Acad. Sci. USA* **107**, 10184–10189 (2010).
41. Coles, C. *et al.* p53 mutations in breast cancer. *Cancer Res.* **52**, 5291–5298 (1992).

ONLINE METHODS

Generation of mice carrying a *Map2k7^{floxed}* allele. A targeting vector was constructed by PCR amplification of a BAC clone carrying the *Map2k7* locus. A 3.5-kb-long arm encompassing exon 2 was isolated with HindIII (H) and cloned downstream of the DTA cassette followed by a HindIII-BamHI (B)-digested middle arm spanning exons 3–10. The short arm (exons 12 and 13) was PCR-amplified and placed downstream of the *Neo* cassette. The construct was linearized and electroporated into A9 embryonic stem cells derived from a 129×C57Bl6 mixed strain. After germline transmission, mice were crossed to Flp transgenic mice to delete the frt-flanked *Neo* cassette. To generate mice carrying a null allele of *Map2k7* (*Map2k7*$^{\Delta}$ allele), *Map2k7*^{floxed} mice were crossed to β-actin-Cre ubiquitous deleter mice. Mice carrying the *Map2k7*^{floxed} or *Map2k7*$^{\Delta}$ alleles as well as the KRas^{G12D} knockin mice[12] were backcrossed at least ten times onto a C57Bl6 background before generating the KRas; *Map2k7*$^{\Delta/floxed}$ mice. MMTV-NeuT mice[42] as well as MMTV-Cre mice[43] have been previously described. Super p53 mice[44] were kindly provided by M. Serrano. JNK1 and JNK2 knockout mice were provided by E. Wagner and have been described previously[45,46]. MMTV-Cre mice[43] (stock # 003553) and *Trp53*^{tm1Tyj} homozygous (p53$^{-/-}$) knockout mice[47] were obtained from the Jackson Laboratory. Mouse genotypes were determined by PCR and DNA blot analysis. In all experiments described in this paper, only littermate mice from the same breeding were used. All mice were bred and maintained according to an ethical animal license protocol complying with the current Austrian law.

Induction of lung tumorigenesis in *Lox-Stop-Lox KRas^{G12D}* mice. Infection of lungs with AdCre was performed as previously described[12]. Briefly, mice were anesthetized with Ketasol/Xylasol and placed on a heated pad. An AdCre-$CaCl_2$ precipitate was produced by mixing 60 µl MEM, 2.5 µl AdCre (10^{10} pfu/ml; University of Iowa, Gene Transfer Vector Core Iowa, USA) and 0.6 µl $CaCl_2$ (1 M) for each mouse and incubated for 20 min at room temperature (21–22 °C). AdCre was administered through intranasal instillation.

Histology, whole-mount analysis and immunohistochemistry. For histological analysis of lung tumors, 4-µm sections from at least three different central planes of the lungs were cut, stained with hematoxylin and eosin and scanned with a Mirax slide scanner. Tumor volume was automatically scored by an algorithm programmed and executed using the definiens software suite program and visually controlled by a pathologist in a blinded fashion. Whole-mount staining of mammary glands was performed as described[48]. For immunoperoxidase staining, paraffin-embedded sections were dehydrated and antigenic epitopes exposed using a 10-mM citrate buffer and microwaving. Sections were incubated with rabbit polyclonal anti-Ki67 (Novocastra), anti-active caspase 3 (Cell Signaling #9661) or anti-MKK7 (Cell Signaling #4172). Primary antibody staining was visualized using peroxidase-conjugated anti-rabbit IgG. Immunohistochemistry for DDR markers was performed as described[15] using the UltraVision LP Detection System (#TL-060-HD, Thermo Scientific, Bioanalytica) according to the manufacturer's instructions, with a modification in the heat-mediated antigen retrieval method. Unmasking of the related proteins was carried out in a 10-mM citrate solution (pH 6.0) for 50 min at 95 °C in a steamer. The following antibodies were used: anti-phospho-H2AX (Ser139, #05-636, Millipore, Lab Supplies) at dilution 1:500; anti-phospho-CHK2 (Thr68, #NB100-92502, Novus Biologicals) at dilution 1:200; and anti-p53 (PAb1620, #ab16776, Abcam, Antisel) at dilution 1:20; p16 (sc-1661 Santa-Cruz), yH2AX (#05-690 Millipore). Primary antibody staining was detected using peroxidase-conjugated anti-rabbit IgG. Expression of γH2AX, CHK2-pT68 and p53 was evaluated as previously described[15]. An average of 500 cells were counted for each antibody and for each section at ×400 magnification. For γH2AX, CHK2-pT68 and p53, a labeling index (%) was calculated, based on the proportion of positive nuclei in the 500 counted cells. Antibodies of the corresponding immunoglobulin class but of unrelated specificity were used as negative controls. Three independent observers carried out slide examination. Inter-observer variability was minimal.

Isolation and culture of primary pneumocytes. Primary pneumocytes were purified as described[49]. Briefly, lungs were removed from 6-week-old mice, infliltrated with dispase through the trachea, incubated for 30 min at room temperature and then manually minced and sequentially passed through a 70 µm and a 35 µm filter to obtain single-cell suspensions. Cells were washed in minimum essential medium (MEM) and red blood cells were lysed using Red Blood Cell Lysis Buffer. Macrophages were removed by plating the cells on mouse IgG (0.5 mg/ml)-coated petri dishes at 37 °C for 1 h. Non-adherent cells were pelleted, resuspended in MEM supplemented with 10% FCS and plated on 10 cm cell culture dishes for the removal of fibroblasts. Non-adherent cells were then plated on collagen-coated 6 cm dishes (160 µg per 6 cm; Collagen Solution (Type I, #C3867 Sigma) for 2 h at room temperature) in Ham's F-12 media supplemented with 15 mM HEPES, 0.8 mM $CaCl_2$, 0.25% BSA, ITS (Sigma) and 2% BSA.

Isolation and culture of primary mammary epithelial cells. Primary mammary epithelial cells were purified as described[50]. Briefly, mammary fad pads were removed from 8-week-old females, manually minced and digested using a collagenase and trypsin solution (DMEM/F12, 0.2% collagenase type IV, 0.2% trypsin, 5% FCS, 5 µg/ml insulin and 50 µg/ml gentamycin) for 30 min on a shaker (350 r.p.m., 37 °C). Cells were washed twice by centrifugation and resuspension in 10 ml DMEM/F12 followed by a DNAse digest (40 µl of DNase (2 U/µl) in 4 ml of DMEM/F12 for 10 min at room temperature). Mammary organoids were separated from single cells by differential centrifugation and seeded onto Growth Factor Reduced Matrigel (BD) overlaid with growth medium (DMEM/F12, ITS supplement (Sigma), 5 ng/ml EGF, 50 µg/ml gentamycin, penicillin and streptomycin). After 3 days, cultures were treated with dispase (BD, 354235) and organoids were seeded in growth medium plus 2% FCS in 10-cm tissue culture plates.

Protein blotting. Protein blotting was carried out using standard protocols. Briefly, blots were blocked with 5% BSA in 1 × TBS 0.1% Tween-20 (TBST) for 1 h and incubated with the primary antibody overnight at 4 °C (diluted in TBST according to the manufacturer's protocol). Primary antibodies were reactive to mouse MKK7 (#4172), MKK4 (#3346), phosphorylated (P) JNK (#9255), JNK (#9252; detecting JNK1 and JNK2), phosphorylated (P) cJun (#9164), cJun (#9162), phosphorylated (P) Akt (#3787), Akt (#9272), phosphorylated (P) Erk1/2 (#9101), Erk1/2 (#9102), p38-MAPK (#9212), p53 (#2524), phosphorylated (P) CHK1 (#2348), CHK1 (#2345), phosphorylated (P) CHK2 (#2197), CHK1 (#2662), phosphorylated (P) Ser(392) p53 (#9281), phosphorylated (P) Ser(15) p53 (#9284), phosphorylated (P) Ser(6) p53 (#9285), phosphorylated (P) Ser(33) p53 (#2526), phosphorylated (P) Thr(81) p53 (#2676) (all from Cell Signaling), p38-MAPK (AF869; R&D), γH2AX (Ser139 #07-164 Millipore) and β-actin (Sigma). Blots were washed three times in TBST for 30 min, incubated with HRP-conjugated secondary antibodies (1:2,000; Promega) for 1 h at room temperature, washed 3 times in TBST for 30 min and visualized using enhanced chemiluminescence (ECL). The JNK kinase assay (#9810) and phospho (P) cJun ELISA Kit (#7145) were from Cell Signaling.

qRT-PCR. Total RNA of tumors was prepared using the RNeasy Mini Kit (QIAGEN) according to the manufacturer's instructions. Total RNA (2 µg) was transcribed into complementary DNA (Amersham Kit) and subjected to quantitative RT-PCR analysis. The primer sequences are given in **Supplementary Table 1**.

siRNA- and short hairpin (shRNA)-mediated gene knockdown of MKK7. For knockdown experiments ON-TARGETplus SMARTpool for MAP2K7 (MKK7) from Dharmacon was used (#L-004016-00). Srcambled siRNA was used as a control. For stable knockdown, hairpin primers used for cloning into pSIREN following the manufacturer's guidelines are given in **Supplementary Table 2**.

DNA damage responses. For measurement of cell cycle arrest and apoptosis primary mouse mammary epithelial cells and A549 human lung cancer cells were seeded at a cell density of 100,000 cells per well in a 6-well plate and allowed to grow for 24 h at 3% O_2. Cells were then treated with doxorubicin or γ-irradiation. Cell cycle distribution was determined by fluorescence-activated cell sorting (FACS) using ethidium bromide (EtBr) staining.

Statistics. All values in the paper are given as means ± s.e.m. Comparisons between groups were made by Student's *t*-test. For the Kaplan Meier

analysis of tumor onset, a log rank test was performed. $P < 0.05$ was accepted as statistically significant.

42. Boggio, K. *et al.* Interleukin 12–mediated prevention of spontaneous mammary adenocarcinomas in two lines of Her-2/neu transgenic mice. *J. Exp. Med.* **188**, 589–596 (1998).
43. Wagner, K.U. *et al.* Cre-mediated gene deletion in the mammary gland. *Nucleic Acids Res.* **25**, 4323–4330 (1997).
44. García-Cao, I. *et al.* "Super p53" mice exhibit enhanced DNA damage response, are tumor resistant and age normally. *EMBO J.* **21**, 6225–6235 (2002).
45. Sabapathy, K. *et al.* c-Jun NH2-terminal kinase (JNK)1 and JNK2 have similar and stage-dependent roles in regulating T cell apoptosis and proliferation. *J. Exp. Med.* **193**, 317–328 (2001).
46. Sabapathy, K. *et al.* JNK2 is required for efficient T-cell activation and apoptosis but not for normal lymphocyte development. *Curr. Biol.* **9**, 116–125 (1999).
47. Jacks, T. *et al.* Tumor spectrum analysis in p53-mutant mice. *Curr. Biol.* **4**, 1–7 (1994).
48. Kim, N., Odgren, P.R., Kim, D.K., Marks, S.C. Jr. & Choi, Y. Diverse roles of the tumor necrosis factor family member TRANCE in skeletal physiology revealed by TRANCE deficiency and partial rescue by a lymphocyte-expressed TRANCE transgene. *Proc. Natl. Acad. Sci. USA* **97**, 10905–10910 (2000).
49. Bortnick, A.E. *et al.* Identification and characterization of rodent ABCA1 in isolated type II pneumocytes. *Am. J. Physiol. Lung Cell. Mol. Physiol.* **285**, L869–L878 (2003).
50. Fata, J.E. *et al.* The MAPK(ERK-1,2) pathway integrates distinct and antagonistic signals from TGFalpha and FGF7 in morphogenesis of mouse mammary epithelium. *Dev. Biol.* **306**, 193–207 (2007).

doi:10.1038/ng.767